Journal of Power Sources 245 (2014) 739–744

Contents lists available at SciVerse ScienceDirect

Journal of Power Sources

journal homepage: www.elsevier.com/locate/jpowsour

Electrochemical activity of carbon blacks in $LiPF_6$-based organic electrolytes

Jarosław Syzdek [a], Marek Marcinek [a,b], Robert Kostecki [a,*]

[a] Environmental Energy Technologies Division, Lawrence Berkeley National Laboratory, Berkeley, CA 94720, USA
[b] Faculty of Chemistry, Warsaw University of Technology, 00-664 Warsaw, Poland

HIGHLIGHTS

- Carbon black additives are electrochemically active toward organic carbonate electrolytes.
- Anion intercalation is the main cause of carbon particles breaking up.
- Electrolyte oxidation processes on carbon black occur at high electrochemical potentials.
- Degradation of carbon additive contributes to gradual loss of power and charge capacity in Li-ion cells.

ARTICLE INFO

Article history:
Received 24 May 2013
Received in revised form
4 July 2013
Accepted 5 July 2013
Available online 14 July 2013

Keywords:
Li-ion battery
Positive electrode
Carbon black
Degradation

ABSTRACT

Electrochemical behavior of carbon black (CB) additives in 1 M $LiPF_6$ EC/DEC (3:7 vol.) electrolyte in the operation potential range of positive electrodes in Li-ion cells was investigated. Various carbon blacks display noticeable electrochemical activity towards PF_6^- intercalation and electrolyte oxidation at potentials >4.0 V vs. Li/Li^+. *In situ* X-ray diffraction, Raman spectroscopy, and *ex situ* scanning electron microscopy and Fourier Transform Infrared (FTIR) spectroscopy showed that repetitive intercalation/deintercalation of PF_6^- anions leads to structural alteration and degradation of carbon black nanoparticles. The mechanism of these interfacial processes on CB electrodes and their implications for electrochemical performance of high-voltage Li-ion electrodes during long-term cycling is evaluated.

© 2013 Elsevier B.V. All rights reserved.

1. Introduction

Li-ion batteries are complex, multi-component electrochemical systems that incorporate widely dissimilar phases in intimate physical and electrical contact. Electronic and ionic transfer across solid–solid, solid–liquid interfaces, and within each of the constituent phases, determines the behavior of composite electrodes as well as the electrochemical performance of the entire cell. Continuous charge–discharge and/or prolonged storage of Li-ion cells invariably lead to a performance degradation caused by irreversible interfacial processes, structural and chemical changes of the electrode active material, and alterations of the composite electrode morphology and topology. The exact mechanism of these complex interrelated processes and their impact on the cell electrochemical performance has not yet been fully understood.

Composite electrodes in lithium-ion cells typically consist of an active material, conductive carbon additive(s), and a binder. Surface reactions, structural degradation and carbon additive distribution changes may alter the electronic properties of the conductive carbon matrix and lead to the loss of electrochemical performance of composite electrodes [1,2]. In fact, carbon black (CB) additives constitute 80–98% of the composite electrode surface area, but very little is known about their electrochemical activity and possible contribution to the electrode and system operation and degradation mechanism.

The electrochemical intercalation of anions into carbons has been studied less extensively than the cation intercalation, and the majority of these studies focused on graphite or graphitic carbons. These investigations indicate that highly oxidizing graphite intercalated compounds (GIC) react with non-aqueous electrolytes, and that co-intercalation of organic carbonates with PF_6^- anion destroys

* Corresponding author.
E-mail address: r_kostecki@lbl.gov (R. Kostecki).

0378-7753/$ – see front matter © 2013 Elsevier B.V. All rights reserved.
http://dx.doi.org/10.1016/j.jpowsour.2013.07.033

the structure of the graphite [3–15]. *In situ* Raman microscopy of tetraethylammonium (Et_4N^+) and tetrafluoroborate (BF_4^-) electrochemical intercalation/deintercalation in microcrystalline graphite showed BF_4^- intercalation at 4.3 V[1] vs. Li/Li^+ [15]. This process was accompanied by changes in Raman D- and G-bands of graphite, typical for staged carbon intercalated compounds. Electrochemical intercalation of PF_6^- and other similar anions into various carbons were studied for the positive electrode in an all-carbon Li-ion rechargeable cell [8,16–21]. PF_6^- intercalation into graphitic carbons occurs *via* staged phases at potentials above 4.5 V, and the extent of the electrochemical intercalation increases with decreasing d_{002} interplanar distance. In other words, the capacity depends on the crystallinity of graphitic-carbons, and the highest value of 90 mAh g^{-1} was obtained for an almost ideal graphitic structure [16]. However, large expansion of d_{002} interplanar distance from 3.35 to 4.5 Å upon PF_6^- intercalation and non-uniform mass transport rate in polycrystalline graphite induces a significant stress in the graphite crystalline lattice, which leads to gradual structural degradation upon cycling [14].

Apart from the anion intercalation behavior of carbons, there is also a significant surface reactivity as the electrochemical potential of intercalated graphite compounds reaches values outside the electrochemical stability window of the electrolyte. This process is very well known and thoroughly studied for low (<1 V) potentials, where carbon electrodes tend to grow the so-called Solid Electrolyte Interphase (SEI) protective layer [22]. The unique properties of the SEI prevent excessive electrolyte decomposition and make LiC_6-based Li-ion cells feasible. Electrolyte decomposition at high potentials has also been studied on various electrodes, including carbon. However, the rate of electrolyte oxidation exponentially accelerates as the electrochemical potential of the electrode is increased [23].

This work focuses on the electrochemical behavior of carbon black additives in $LiPF_6$-based organic carbonate electrolytes at potentials above 2.5 V i.e., in the voltage range where all positive electrodes operate in Li-ion battery systems. The goal of this study was to understand the mechanism of surface and bulk processes on CB additives and their possible implications for the electrochemical performance of Li-ion cells.

2. Experimental

Three different CB additives were used for composite electrodes preparation: Shawinigan Black® (Chevron Phillips), Denka Acetylene Black (Denki Kagaku Kogyo K.K.) and Super P™ Li (TIMCAL). Two different electrode formulations were used: 90% CB with 10% PVdF (polyvinylidene difluoride), Kynar® binder, and 45% Shawinigan Black, 45% TIMREX® SFG6 graphite (TIMCAL) and 10% PVdF. Composite electrodes have been prepared from *N*-methyl-2-pyrrolidone (Sigma–Aldrich) slurries on an Al current collector (99.9% Al, Sigma–Aldrich) using a standard doctor blade procedure. Electrode thickness was 2.5 μm; loading was approximately 0.1 mg of carbon per cm^2, which corresponds roughly to a typical carbon loading in commercial Li-ion electrodes. Freshly prepared electrodes were dried in a He-filled glove box antechamber vacuum oven (OC-1R, Vacuum Atmospheres) at 0.6 Pa, 120 °C for 72 h. Dry electrodes were transferred directly into the glove box (H_2O and O_2 levels <0.1 ppm). 12 mm dia. disc electrodes were used for electrochemical tests.

A Gamry600 potentiostat was used to cycle the electrodes 2000 times between 2.5 and 4.9 V at 1 mV s^{-1} in 1 M $LiPF_6$ EC/DEC (3:7 vol.) (Novolyte) in coin cells (2032) with a Li-foil counter electrode (Sigma Aldrich, >99.9%) at room temperature (RT) and 45 °C. Some electrodes were also aged in the electrolyte at room temperature for two months.

A Raman microscope system "Labram" (ISA Group Horiba) was used to analyze the electrode surface structure and composition. The excitation source was a 20 mW He–Ne laser (632.8 nm). The power of the laser beam was adjusted to 0.1 mW and the diameter of the laser beam at the sample was ~1.2 μm. X-ray diffraction (XRD) measurements were performed with a D8 Bruker diffractometer equipped with a $CuK\alpha_{1,2}$ source in Bragg–Brentano (θ–θ) geometry. SEM imaging was carried out with a Hitachi S-4300 SE/N EDX microscope. Fourier Transform Infrared (FTIR) Attenuated Total Reflection (ATR) spectra were collected using a Ge crystal with a Nicolet Continuum Nexus 870 microscope (Thermo Scientific).

In situ spectro-electrochemical measurements were conducted in an airtight cell that was described in our previous study [24]. The working electrode consisted of a strip of Al current collector 20 mm long and 1.5 mm wide with ~1 mm^2 active area of CB/PVdF film at its end. The electrode was positioned 0.2 mm below the glass window with the CB film facing up, which allowed optical access to the electrode through a thin electrolyte gap. A lithium-foil counter electrode was fixed at the bottom of the cell and covered by a piece of commercial Celgard® 2300 separator. The cell was assembled, filled with the electrolyte, sealed in the glove box, and then transferred to the Raman microscope.

A different cell configuration was used for *in situ* XRD studies. Pure CB powder (10 mg) was tipped onto an Al-coated Be window fixed into a stainless steel body. A 16 mm dia. Celgard® disc was placed on top of the CB powder, soaked with the electrolyte and topped with a 12 mm dia. Li-foil disc attached to a stainless steel current collector. The cell was then sealed with a Swagelok-type Teflon seal.

3. Results

Fig. 1a presents a series of selected voltammograms of a Shawinigan Black electrode recorded during long-term cycling. The initial cycle shows a gradually increasing anodic current starting at *ca.* 3.5 V, with small features at 3.64, 4.04 and 4.51 V, and a sharp current rise at 4.7 V. During the reverse scan the oxidation processes continued until 4.35 V followed by a cathodic peak at 3.55 V. The 5th cycle exhibits slightly smaller oxidation current at high potentials; the peaks at 3.64 and 4.04 V merge into a well-defined red-ox couple at 3.7 V whereas the peak at 4.51 V disappears. During the reverse scan the current changes sign to negative at a higher potential (~4.6 V). The 10th cycle features predominantly positive currents throughout most of the scan and the negative shift of the red-ox couple to 3.5 V. The 20th scan reveals double red-ox features at 3.45 and 3.55 V, which then diminish in intensity in the following cycles. The anodic current at high potentials follows a similar trend. The current response in cycle #2000 becomes purely capacitive and featureless with the exception of the overlaying electrolyte oxidation current at ($E > 4.65$ V). Such electrochemical behavior was observed consistently (with some degree of variation) for Super P, and Denka carbon black electrodes.

Fig. 1b shows a similar set of voltammograms obtained for a mixed Shawinigan Black/SFG6 electrode. The first cycle shows small anodic features at 3.9 and 4.2 V and a strong anodic peak at 4.8 V followed by a series of cathodic peaks at 4.7, 4.5, 4.2, 4.0 and 3.9 V at a relatively strong oxidation current background during the reverse scan. The following CV plots are dominated by two overlapping anodic peaks at 4.66 and 4.77 V, and cathodic features at 4.65, 4.47, 4.19 and 3.89 V, which originate from PF_6^- intercalation/deintercalation in graphite [3]. As the cycling progresses the

[1] All electrochemical potentials in this work are given with respect to the Li/Li^+ reference electrode.

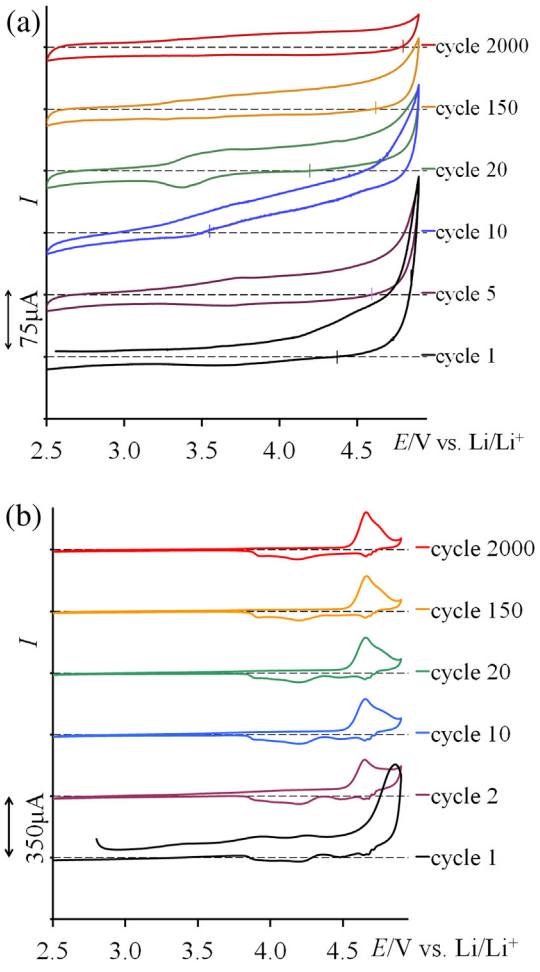

Fig. 1. Cyclic voltammograms of (a) Shawinigan Black and (b) Shawinigan Black/SFG6 graphite composite electrode in 1 M $LiPF_6$ EC/DEC 3:7 (vol.) electrolyte. Scan rate: 1 mV s^{-1}, Li-foil counter electrode.

capacitive current background and the intensity of electrolyte oxidation at high potentials diminish without any significant change of the PF_6^- intercalation/deintercalation peak positions.

Interestingly, Coulombic efficiency of the CV cycles grows from as little as 17% and 4.4% in cycle #1 to 70% and 73% in cycle #2000 for CB and CB/graphite electrodes, respectively. The permanent imbalance of anodic and cathodic charge consumed on carbon electrodes during long-term CV cycling indicates that irreversible electrolyte oxidation processes dominate the electrochemical behavior of the CB electrodes, which may have quite severe implications for the lifetime of high-voltage Li-ion battery systems.

Ex situ Raman microscopy was used to assess structural changes in the Shawinigan Black carbon electrode that was cycled 150 times between 2.5 and 4.9 V at 1 mV s^{-1} in a coin cell at room temperature and 45 °C. Thousands of Raman spectra collected from a 52 × 75 μm section of the CB electrode at 0.9 μm spatial resolution were baseline corrected and averaged into one representative spectrum for the whole area (Fig. 2). The Raman spectra of the carbon black consist of a G-band at 1580 cm^{-1} corresponding to the E_{2g} active mode of graphite and the D-band located at 1322 cm^{-1} that is assigned to the A_{1g} mode, and associated with the breakage of symmetry that occurs at the edges of graphite sheets [25]. D/G peak integrated intensity ratio is strongly correlated with the size of graphitic domains in the material and the amount of structural defects [26].

Upon prolonged electrochemical cycling of the carbon black electrode the D/G peak ratio increased from 0.641 for fresh to 0.687

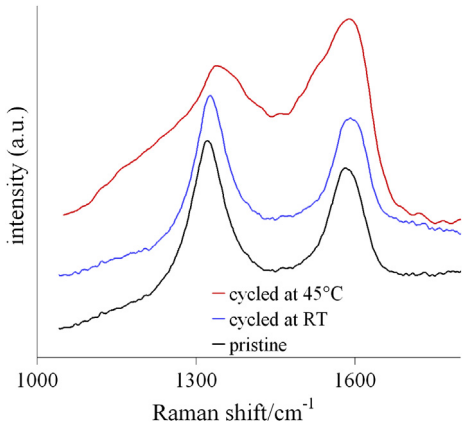

Fig. 2. Averaged *ex situ* Raman spectra of Shawinigan Black electrodes: fresh, cycled at room temperature (RT) and 45 °C (2000 cycles between 2.5 and 4.9 V at 1 mV s^{-1}).

and 1.20 for the CB electrode cycled at room temperature and 45 °C, respectively. Furthermore, the peak positions shift from 1322 to 1343 cm^{-1}, and from 1580 to 1593 cm^{-1}, for the D- and G-bands, respectively, and they broaden by ~33% during cycling at 45 °C. The D/G ratio increase and peak broadening are usually associated with an increase in the number of structural defects and/or decrease of the size of graphene domains in the material [27]. The observed structural degradation of carbon black that occurs during cycling in the electrolyte appears to be greatly accelerated at elevated temperatures.

Fig. 3 shows *ex situ* SEM micrographs of fresh and cycled Shawinigan Black electrodes at room temperature and 45 °C at two different magnifications. Substantial changes of the particle and electrode surface morphology after prolonged cycling were observed, especially for the CB electrode cycled at 45 °C. Densely packed 80–100 nm CB particles in the fresh electrode are nearly double in size in the electrode cycled at 45 °C. On the other hand, the cycled electrodes exhibit increased surface porosity due to possible loss of the carbon material. The CB particle swelling can be related to the observed carbon structural degradation and possible intercalation and entrapping of PF_6^- anions in between disordered graphene sheets. No evidence of a surface film of electrolyte oxidation products was observed in the SEM images of cycled electrodes, which most likely were washed off in DEC prior to imaging.

Fig. 4 presents *ex situ* ATR-FTIR spectra of the pristine Shawinigan Black electrode that was briefly exposed to the electrolyte (1 min), electrode aged in the electrolyte for two months at room temperature, and the electrode that was cycled 2000 times between 2.5 and 4.9 V at 1 mV s^{-1} at room temperature (all samples were pat-dried; no DEC washing was applied). All spectra display bands characteristic for the PVdF binder, i.e., C–H wagging mode at 1395 cm^{-1}, C–F symmetric stretching at 1232 and 872 cm^{-1} and mixed C–F asymmetric stretching and CH_2 rocking vibrations at 840 cm^{-1} [28].

The ATR-FTIR spectra also exhibit strong evidence of electrolyte decomposition products and EC and $LiPF_6$ residues. The cycled and aged electrodes show a series of IR bands at 1806, 1774, and 1732 cm^{-1} that are characteristic for alkyl carbonates RCO_2Li (>C=O stretching). The C=O symmetric stretching band at 1620 cm^{-1} belongs to lithium ethylene dicarbonate [29–31] and C–O asymmetric stretching band at 1072 cm^{-1} can be assigned to lithium methoxide $LiOCH_3$ [32]. The later band can be also assigned to a similar C–O stretching vibration from carbonate ethers and/or PEO [33–35].

All the ATR-FTIR spectra indicate the presence of PF_6^- and its inorganic decomposition products with the relevant P–F bands at

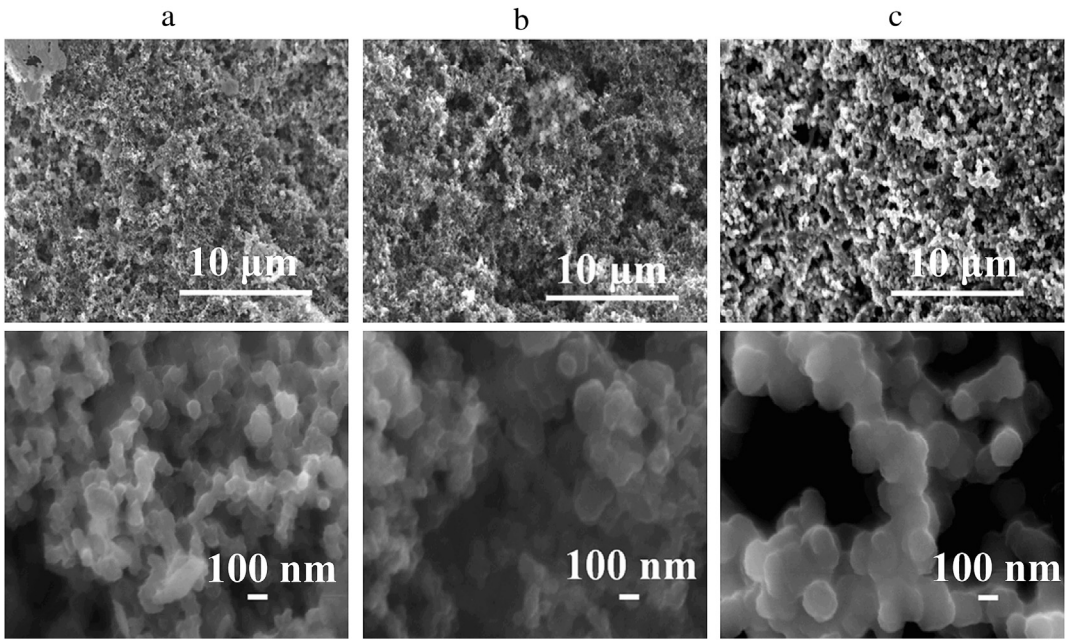

Fig. 3. *Ex situ* SEM micrographs of Shawinigan Black electrodes: (a) fresh, (b) cycled at RT, (c) cycled at 45 °C (2000 cycles between 2.5 and 4.9 V at 1 mV s^{-1}).

840 and 905 cm^{-1}, and the P–O symmetric stretch vibration at 1115 cm^{-1} [36–38]. The band at 751 cm^{-1} is most likely associated with C–O and/or P–O bending modes [39]. The observed differences in FTIR spectra of the fresh, aged and cycled electrodes indicate that surface films form almost immediately upon contact with the electrolyte. The film composition and thickness changes significantly upon prolonged storage or cycling in the electrolyte. However, the increased intensity of the band at 840 cm^{-1} in the cycled electrode FTIR spectrum may be indicative of PF_6^- anions intercalated into carbon black.

In situ Raman microscopy was used to monitor structural changes in carbon black during the first CV scan (Fig. 5). The relative intensity of carbon D- and G-bands, which are clearly visible at 3.3 V starts to diminish at 4.2 V and these bands almost completely disappear at 4.8 V. The bands intensity variations are accompanied by significant band broadening during the cathodic scan. Remarkably, both carbon bands were restored during the reverse scan at potentials below 3.5 V. On the other hand, a large gap between the potentials at which carbon Raman bands disappear and reappear suggests significant kinetic limitations in this material. Only partial restoration of the initial spectrum suggests that this process is not fully reversible, and PF_6^- anions get trapped in the CB structure. Broadening of the D- and G-bands at the end of the cycle may also suggest structural changes/degradation of the host carbon black material. Such spectral behavior has been commonly observed upon formation and decomposition of graphite intercalation compounds [15]. The characteristic G-band doublet peak ($E_{2g2(i)}$ (1578 cm^{-1}) and $E_{2g2(b)}$ (1600 cm^{-1})) followed by the band collapse showed that various staged compounds were formed, and the return of the single G-band (1578 cm^{-1}) upon deintercalation demonstrates that the process is fully reversible. The disappearance of the D-band (1329 cm^{-1}) in GICs is also typical but when the ions

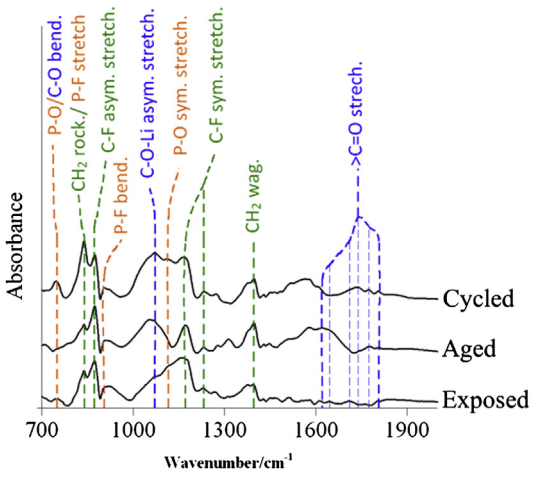

Fig. 4. *Ex situ* FTIR spectra of a Shawinigan Black electrodes: after brief (1 min) exposure to the electrolyte, aged in the electrolyte for two months at room temperature, and cycled 2000 times between 2.5 and 4.9 V at 1 mV s^{-1} at room temperature.

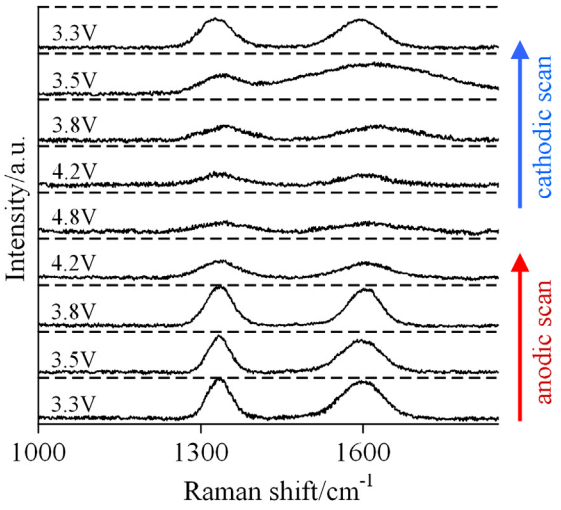

Fig. 5. *In situ* Raman spectra of the Shawinigan Black electrode during the first CV scan between 2.5 and 4.9 V at 1 mV s^{-1}.

are removed from the lattice an increased intensity of the D-band reappears suggests graphite lattice damage.

In situ XRD provided further insight into the observed phenomenon. Diffraction patterns were recorded for a freshly assembled cell (OCV = 2.9 V), after the potential was scanned to 4.9 V, and finally after 2000 CV cycles between 2.5 and 4.9 V at 1 mV s^{-1} at room temperature (Fig. 6a). Diffractograms intensity and zero-shift were normalized vs. reflections from inert cell components i.e., Be window and steel casing. Gaussian function was used for diffraction peak fitting. Single charge didn't produce much of a change of the d_{002} spacing (shift from 3.474 Å to 3.478 Å). However after 2000 cycles the position and shape of graphite d_{002} diffraction peak changed quite significantly, which again indicates structural modifications of CB upon cycling. In fact, the average d_{002} spacing increased to 3.562 Å, which was deducted from the numerical fit of the data shown in Fig. 6b and c (CB (002) reflection plotted in blue in web version). Moreover, the half-width of the d_{002} reflection increased upon cycling by *ca.* 83%, indicating possible fracture of carbon grains, presence of graphitic domains with significantly higher (002) spacing and induced stress. These structural degradation processes can lead to a serious distortion of the CB additive function and operation in high-voltage composite Li-ion electrodes.

4. Discussion

Carbon black particles typically consist of disordered graphitic domains with varying orientation and the d_{002} spacing that is usually greater than in graphite (3.35 Å). These domains contain a lot of voids and point defects; nonetheless the ion intercalation mechanism should be similar to graphite. In fact, the small size of graphitic domains and larger d_{002} spacing should facilitate anion intercalation and bring the reaction potential well below 4.5 V.

In order to satisfy charge balance/conservation, carbon has to release electrons upon anion intercalation. That leads to PF_6^- anions creating a fairly strong bond with positively charged graphene planes, which changes the local composition/symmetry and the electronic band structure of the intercalated compound. The PF_6^-–C bond weakens the π-bond of the C^+ atom and its C° neighbor, the bond length increases and causes the C^+ atoms to "pop up" from the graphene plane, creating an anti-symmetrical bi-pyramidal structure [40]. These phenomena contribute to the displacement of charged atoms, destroy planarity of the graphene sheet and increase its corrugated character. The collapse of carbon Raman bands upon PF_6^- intercalation (similarly to Li^+ intercalation in graphite) can be explained by the increasing number of "misplaced" carbon atoms, which distort the local symmetry and inhibit propagation of the "in-plane" E_{2g} vibration mode.

Steele and Dahn [14] postulated that ordered hexagonal superstructures for intercalated anions occur in graphite at compositions of AC_6, AC_8, AC_{14}, AC_{18}, etc. The d_{002} spacing in graphite increases by 34% upon PF_6^- intercalation, which induces a significant stress into the structure and leads to graphene planes breakdown and structural degradation. Thus the observed gradual structural degradation of the CB electrode upon cycling is most likely caused by a similar effect. Moreover, because of the short-range order in carbon black particles, even small amount of intercalated anions can induce significant displacement and structural rearrangement of graphene planes and possible permanent entrapment of anions in the structure. The eventually may lead to particle swelling and possible breaking up.

This structural degradation process is aggravated by the electrolyte oxidation that produces a thin surface layer of organic and inorganic electrolyte decomposition products. Considering the fact that carbon additives constitute >80% of the composite electrode surface area, the charge consumed in these side reactions may be responsible for the observed long-term lithium inventory shift in Li-ion cells, which contributes to the mechanism of battery failure. Moreover, such a surface film on the CB conductive additive creates electronic and ionic barriers and affect the electron transfer and

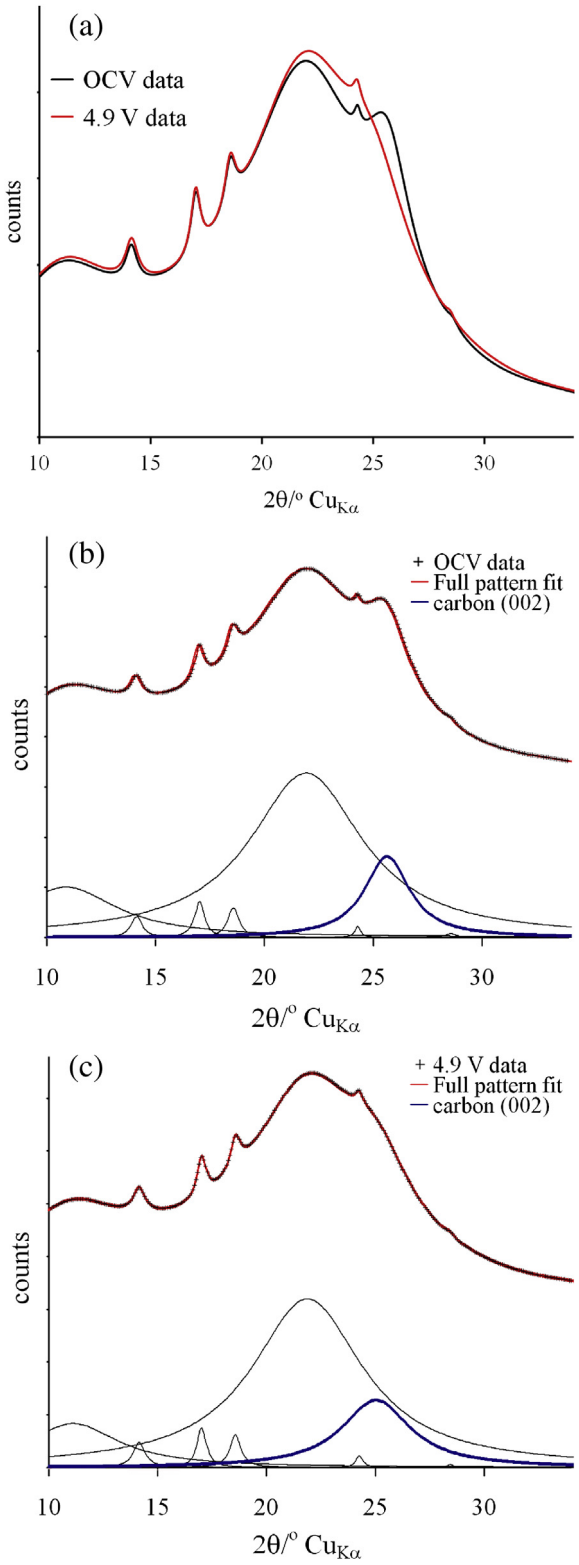

Fig. 6. *In situ* XRD patterns of fresh and cycled Shawinigan Black (2000 cycles between 2.5 and 4.9 V at 1 mV s^{-1} at room temperature) (a), and the corresponding experimental data fitting (b) and (c) (black traces in (b) and (c) correspond to contributions from cell components i.e., steel case, polymer separator, liquid electrolyte etc.).

mass transport, which contribute to the universally observed impedance rise and capacity loss in the composite electrodes in Li-ion cells [1,41–45]. A simple theoretical model based on a distributed network confirmed that a local increase of the contact resistance between composite electrode active and passive particles can alter distribution of the conductive paths, and consequently, lead to a significant increase of the mid-frequency semi-circle in the impedance spectra with a minimal effect on the position of the high-frequency intercept [36].

5. Conclusions

All types of carbon black additives appear to be electrochemically active toward $LiPF_6$ based organic carbonate electrolytes at potentials at which most Li-ion positive electrodes operate (>4 V). The PF_6 intercalation into CB occurs at potentials significantly lower than for PF_6^- intercalation in graphite (~4.5 V), which is assigned to larger d_{002} spacing in CB than in graphite. This process is not fully reversible and constitutes the main cause of morphological and structural changes of carbon material, leading to possible changes in its structure, morphology and electronic properties. It is the main cause of carbon particles breaking up and gradual loss from the composite electrodes.

The spectro-electrochemical investigations also reveal electrolyte oxidation processes on carbon black at high electrochemical potentials. Electrolyte degradation products precipitate at the surface of carbon black, and contribute to the buildup of ionic and electronic barriers within the electrode. It decreases carbon electronic conductivity and increases contact resistance between carbon and active material. The observed electrochemical activity of carbon blacks in organic electrolytes at high potentials contributes to the gradual loss of power and charge capacity in Li-ion electrodes operating at high potentials. The structural properties and distribution of carbon conductive additives for high voltage positive electrodes must be carefully optimized and matched to expected cycling potential range and electrolyte chemistry in order to provide reliable long-term electrochemical performance and safe operation.

Acknowledgment

This work was supported by the Assistant Secretary for Energy Efficiency and Renewable Energy, Office of Vehicle Technologies of the U.S. Department of Energy under Contract No. DE-AC02-05CH11231.

References

[1] M. Kerlau, R. Kostecki, J. Electrochem. Soc. 153 (2006) A1644–A1648.
[2] L. Fransson, T. Eriksson, K. Edström, T. Gustafsson, J.O. Thomas, J. Power Sources 101 (2001) 1–9.
[3] J.O. Besenhard, H.P. Fritz, Z. Naturforsch. B27 (1972) 1294–1298.
[4] M.B. Armand, in: Fast Ion Transport in Solids, Solid State Batteries Devices, Proceedings of the NATO Sponsored Advanced Study Institute, 1973, pp. 665–673.
[5] M.B. Armand, Ger. Offen., 73-2341723, 1974, 42.
[6] J.O. Besenhard, H.P. Fritz, Z. Anorg. Allg. Chem. 416 (1975) 106–116.
[7] D. Billaud, A. Pron, F. Lincoln Vogel, A. Hérold, Mater. Res. Bull. 15 (1980) 1627–1634.
[8] F. Beck, H. Junge, H. Krohn, Electrochim. Acta 26 (1981) 799–809.
[9] D. Billaud, A. Chenite, A. Metrot, Carbon 20 (1982) 493–497.
[10] A. Chenite, A. Metrot, D. Billaud, A. Herold, Synth. Met. 7 (1983) 201.
[11] P. Touzain, A. Jobert, Bull. Soc. Chim. Fr. 5-6 (1983) I110.
[12] R. Santhanam, M. Noel, J. Power Sources 66 (1997) 47–54.
[13] H.P. Boehm, B. Ruisinger, in: Extended Abstracts, 17th Biennial Conference on Carbon, 1985, pp. 57–58.
[14] J.A. Steele, J.R. Dahn, J. Electrochem. Soc. 147 (2000) 892.
[15] L.J. Hardwick, M. Hahn, P. Ruch, M. Holzapfel, W. Scheifele, H. Buqa, F. Krumeich, P. Novák, R. Kötz, Electrochim. Acta 52 (2006) 675–680.
[16] T. Ishihara, M. Koga, H. Matsumoto, M. Yoshio, Electrochem. Solid State Lett. 10 (2007) A74–A76.
[17] F.P. McCullough, A. Levine, R.V. Snelgrove, U.S. Patent 4,830,938, 1989.
[18] J.O. Besenhard, H.P. Fritz, Angew. Chem. Int. Ed. Engl. 22 (1983) 950–975.
[19] H. Zaleski, P.K. Ummat, W.R. Datars, Solid State Commun. 55 (1985) 401–403.
[20] H. Zaleski, P.K. Ummat, W.R. Datars, Synth. Met. 11 (1985) 183–191.
[21] W. Rudorff, U. Hofmann, Z. Anorg. Allg. Chem. 238 (1938) 1–50.
[22] E. Peled, J. Electrochem. Soc. 126 (1979) 2047–2051.
[23] K. Xu, Chem. Rev. 104 (10) (2004) 4303–4418.
[24] J. Lei, F. McLarnon, R. Kostecki, J. Phys. Chem. B 109 (2005) 952–957.
[25] G. Katagiri, H. Ishuda, A. Ishitani, Carbon 26 (1988) 565–571.
[26] F. Tuinstra, J.L. Koenig, J. Chem. Phys. 53 (1970) 1126–1130.
[27] E. Pollak, B. Geng, K. Jeon, I.T. Lucas, T.J. Richardson, F. Wang, R. Kostecki, Nano Lett. 10 (2010) 3386–3388.
[28] M.A. Bachmann, J.L. Koenig, J. Chem. Phys. 74 (1981) 5896–5910.
[29] D. Aurbach, B. Markovsky, A. Schechter, Y. Ein Eli, J. Electrochem. Soc. 143 (1996) 3809–3820.
[30] G.V. Zhuang, K. Xu, H. Yang, T.R. Jow, P.N. Ross, J. Phys. Chem. B 109 (2005) 17567–17573.
[31] K. Xu, G.V. Zhuang, J.L. Allen, U. Lee, S.S. Zhang, N. Ross Philip, T.R. Jow, J. Phys. Chem. B 110 (2006) 7708–7719.
[32] G.V. Zhuang, H. Yang, B. Blizanac, P.N. Ross, Electrochem. Solid State Lett. 8 (2005) A441–A445.
[33] D. Aurbach, B. Markovsky, A. Rodkin, M. Cojocaru, E. Levi, H. Kim, Electrochim. Acta 47 (2002) 1899–1911.
[34] K. Tashiro, M. Kobayashi, H. Tadokoro, Macromolecules 14 (1981) 1757–1764.
[35] R. Nyquist (Ed.), Interpreting Infrared, Raman, and Nuclear Magnetic Resonance Spectra, Elsevier, 2001 (Chapter 8).
[36] M. Kerlau, M. Marcinek, V. Srinivasan, R.M. Kostecki, Electrochim. Acta 52 (2007) 5422–5429.
[37] S. Laruelle, S. Pilard, P. Guenot, S. Grugeon, J.-M. Tarascon, J. Electrochem. Soc. 151 (2004) A1202–A1209.
[38] S.E. Sloop, J.B. Kerr, K. Kinoshita, J. Power Sources 119–121 (2003) 330–337.
[39] K. Nakamoto, Infrared and Raman Spectra of Inorganic and Coordination Compounds, 1986.
[40] I. Pocsik, M. Veres, M. Fule, S. Toth, M. Koos, arXiv:cond-mat/0307476v1.
[41] D.P. Abraham, R.D. Twesten, M. Balasubramanian, J. Kropf, D. Fischer, J. McBreen, I. Petrov, K. Amine, J. Electrochem. Soc. 150 (2003) A1450–A1456.
[42] G.V. Zhuang, G. Chen, J. Shim, X. Song, P.N. Ross, T.J. Richardson, J. Power Sources 4 (2004) 293–297.
[43] S.W. Song, G.V. Zhuang, P.N. Ross, J. Electrochem. Soc. 151 (2004) A1162–A1167.
[44] M. Kerlau, J.A. Reimer, E.J. Cairns, J. Electrochem. Soc. 152 (2005) A1629–A1635.
[45] Z. Chen, J.R. Dahn, Electrochem. Solid State Lett. 7 (2004) A11–A14.